The Sparse Matrix-Based Random Projection: A Study of Binary and Ternary Quantization

Anonymous authors
Paper under double-blind review

Abstract

Random projection is a straightforward yet effective dimension reduction technique, widely used in various classification tasks. Following the projection process, quantization is often applied to further simplify the projected data. Typically, quantized projections are required to approximately preserve the pairwise distance between original data points, to avoid significant performance degradation in classification tasks. To date, this distance preservation property has been investigated for the commonly-used Gaussian matrix. In the paper, we further explore this property for the hardware-friendly $\{0, 1\}$-binary matrix, specifically when the projections undergo element-wise quantization into two types of low bit-width codes: $\{0, 1\}$-binary codes and $\{0, \pm 1\}$-ternary codes. It is found that the distance preservation property tends to be better maintained, when the binary projection matrix exhibits sparse structures. This property is corroborated by experiments on both classification and clustering tasks, where extremely sparse binary matrices, with only one nonzero entry per column, demonstrate better or comparable performance compared to other more dense binary matrices and Gaussian matrices. This presents an opportunity to significantly reduce the computational and storage complexity of the quantized random projection model, without compromising and potentially even improving its classification performance.

1 Introduction

Random projection is an unsupervised dimension reduction technique (Johnson & Lindenstrauss, 1984) that simply projects a data vector $x \in \mathbb{R}^n$ from high dimension to low dimension via a linear measurement

$$x' = Rx, \tag{1}$$

where $R \in \mathbb{R}^{m \times n}$ is a random matrix, $m \ll n$. For the random matrices with Gaussian distributions (Dasgupta & Gupta, 1999), sparse $\{0, \pm 1\}$-distributions (Achlioptas, 2003) and $\{0, 1\}$-distributions (Dasgupta et al., 2017; Li & Zhang, 2022), it has been proved that the distance between any two original data points x can be approximately preserved with high probability by their projections. The pairwise distance preservation property implies the approximate preservation of data structure, which enables random projection to be widely used in practical classification problems, while not causing drastic performance degradation.

In large-scale classification, it is common to further impose an element-wise quantization operation $f(x')$ on the random projection x' of original data x, such as the popular $\{0, 1\}$-binary or $\{0, \pm 1\}$-ternary quantization, in order to further reduce the data complexity. This operation results in a *quantized* random projection model, which can be found in many applications and models, such as large-scale retrieval (Charikar, 2002) and deep network quantization (Wan et al., 2018; Qin et al., 2020). For such a quantization model, the major concern remains the pairwise distance preservation property. More precisely, provided two data points u, $v \in \mathbb{R}^n$ and their projections u', $v' \in \mathbb{R}^m$, it is necessary to find a random matrix $R \in \mathbb{R}^{m \times n}$ such that the relation of $\|f(u') - f(v')\| = \|u - v\|$, or equivalently $f(u')^\top f(v') = u^\top v$ for normalized data, holds with high probability. This distance preservation property $f(u')^\top f(v') = u^\top v$ has been analyzed for Gaussian matrices (Charikar, 2002; Li et al., 2014), but not for the sparse $\{0, \pm 1\}$-ternary or $\{0, 1\}$-binary matrices. Nevertheless, sparse matrices are preferred in practice because of their simpler structures. To maximally

simplify the structure of sparse matrices, it is of high interest to estimate their sparsest distribution, namely the minimal number of nonzero entries under the aforementioned distance preservation condition. This proposes a discrete optimization problem, which seems hard to be addressed with the probability analysis method used for Gaussian matrices. In the paper, we show that the problem could be tackled, if the data to be projected have sparse distributions.

The data of sparse distributions are common in signal processing and machine learning. For instance, it is known that the natural data of interest, like images and sounds, usually contain coherent structures and redundant information over spatial or time domains (Ruderman, 1994; Simoncelli, 1999; Weiss & Freeman, 2007; Kotz et al., 2012; Iyer & Burge, 2019), and thus allow to be sparsified via globally or locally linear transforms, such as the discrete cosine transform (DCT) (Rao & Yip, 2014; Eude et al., 1994), the discrete wavelet transform (DWT) (Mallat, 2009), the deep convolutional neural networks (CNN) (Krizhevsky et al., 2012), and so on. In general, the sparse transforms will provide more discriminative features for classification, especially when zeroing out the small-magnitude feature elements caused by high-frequency noise (Zarka et al., 2020). Furthermore, the feature discrimination could be improved further, as the remaining large feature elements are quantized to the values of ± 1 or 1 through appropriate ternary or binary quantization (Lu et al., 2023). This suggests that employing low bit-width binary and ternary quantization on sparse features is advantageous for classification in terms of both complexity and accuracy. Then for the quantized random projection of sparse features, instead of the conventional distance preservation condition of $f(u')^\top f(v') = u^\top v$, we propose the condition of $f(u')^\top f(v') = f^\top(u) f(v)$, i.e. preserving the distance between the quantization codes of sparse features, in order to allow the quantized projections to capture more discriminative features from the original data.

With the quantized sparse features as input, the random projection model is somewhat similar to the compressed sensing model (Donoho, 2006). Inspired by the analysis of the sparse $\{0, 1\}$-binary matrix-based compressed sensing (Mendoza-Smith & Tanner, 2017; Lu et al., 2018), in the paper we investigate the proposed distance preservation property $f(u')^\top f(v') = f^\top(u) f(v)$ for the sparse binary matrix-based random projection. By varying the matrix sparsity, we find that the property tends to be better satisfied by the very sparse matrices which contain only one nonzero entry per column, than other more dense counterparts. Accordingly, theses extremely sparse matrices also achieve better performance in both supervised and unsupervised learning tasks, specifically classification and clustering. This is good news in terms of both complexity and accuracy. Overall, the major contributions of the paper can be summarized as follows.

- For the binary matrix-based random projection, we for the first time study the impact of matrix sparsity on the performance of ternary (and binary) *quantized* projections in the conventional classification and clustering tasks. It is found that the extremely sparse binary matrices that contain only one nonzero entry per column tend to perform better than other more dense matrices, when the original data to be projected are the sparse features we commonly study, such as the DWT and CNN features generated with the known datasets YaleB (Georghiades et al., 2001; Lee et al., 2005), CIFAR10 (Krizhevsky & Hinton, 2009) and ImageNet (Deng et al., 2009).
- To estimate the optimal matrix sparsity, we investigate how accurately the ternary (and binary) quantized projection can preserve the pairwise distance between the ternary (and binary) quantization of original data, rather than directly between the original data as conventionally studied. The proposed distance preservation offers two advantages: firstly, it enables the quantized projection to obtain more discriminative features from the original data, as the data are the sparse features described above (Lu et al., 2023); and secondly, it is suited for the analysis of the binary matrix based quantized random projection, which seems hard to analyze using the conventional distance preservation condition.

The rest of the paper is organized as follows. In the next section, we review the literature related to the quantized random projection model. In Section 3, we introduce the basic knowledge about the model and describe the proposed distance preservation property. Among the binary matrices with different sparsity, the one that better holds the proposed property is estimated in Section 4. The performance advantage of such matrix in classification and clustering is verified in Section 5. Section 6 concludes the work.

2 Related work

The quantized random projection model has been studied in two research areas: local similarity hashing (LSH) (Charikar, 2002; Boufounos & Rane, 2013; Valsesia & Magli, 2016) and compressed sensing (Jacques et al., 2013). The former aims to adopt quantized projections to build hash tables for information retrieval, and the latter aims to reconstruct original data from quantized projections. Different from our work, both of them, broadly speaking, require the quantized projection $f(x')$ to preserve the pairwise distance (or similarity) between original data x, rather than between their quantization versions $f(x)$. Furthermore, their studies are mainly focused on Gaussian matrices. For the classification on quantized projections, a systematic evaluation has been presented in (Li et al., 2014), which demonstrates that compared to unquantized projections, a slight performance reduction inclines to be caused by 2-bit quantization, and the reduction becomes noticeable for 1-bit quantization. Recently, empirical evidence has shown that binary and ternary quantization methods can improve classification accuracy, particularly when dealing with commonly-used sparse features (Lu et al., 2023). Furthermore, when sparse features undergo random projections and classification is conducted on the quantized projections, random projections based on extremely sparse $\{0, \pm 1\}$-matrices tend to achieve better classification performance than those based on Gaussian matrices. This remarkable performance motivates us to deeply investigate the impact of sparse matrices on the classification of quantized projections through theoretical analysis.

For random projections based on sparse matrices, like $\{0, \pm 1\}$-ternary matrices and $\{0, 1\}$-binary matrices, existing research mainly explores the distance preservation property for the linear model (1), without quantization considered. Specifically, the ℓ_2 distance preservation property of ternary matrices has been studied in (Li et al., 2006), which demonstrates that the property can be well satisfied when the matrix has the proportion of nonzero entries greater than $1/\sqrt{n}$. In (Dasgupta et al., 2017), the ℓ_2 distance preservation is analyzed for binary matrices, and empirically the matrices tend to reach a stable performance for nearest neighbors search when containing more than about 10% nonzero entries. In contrast, out study demonstrates that for the quantized projections of sparse features, binary matrices can generally achieve the best classification performance when containing only one nonzero entry per column.

3 Problem Formulation

In the paper, we study the random projection model (1) which has the original data $x \in \mathbb{R}^n$ sparsely distributed and has the random matrix $R \in \{0, 1\}^{m \times n}$ binary distributed. To improve the classification on the quantization of projected data, we present a novel distance preservation property that maintains the pairwise distance between the quantization of original data, rather than between the original data themselves, and then investigate the probability that the property holds for the binary matrix with varying matrix sparsity. In this section we provide the basic knowledge about the study, including the distribution of binary matrices R, the distribution of original data x, the quantization functions $f(\cdot)$, as well as the distance preservation model.

3.1 Binary matrix

For a random binary matrix $R \in \{0, 1\}^{m \times n}$, we assume it contains d ($< m$) nonzero entries per column, or say having column degree d. This parameter measures the matrix sparsity, whose impact on distance preservation will be the core of our research. We denote $R_{i,j} \in \mathbb{R}$ as the entry at the i-th row and j-th column, $R_{*,j} \in \mathbb{R}^m$ the j-th column vector, $R_{i,*} \in \mathbb{R}^{1 \times n}$ the i-th row vector, $R_{i,\phi} \in \mathbb{R}^{1 \times |\phi|}$ the intersection of the i-th row and the columns indexed by $\phi \subset [n]$, $[n] := \{1, 2, ..., n\}$, and $R_{*,\phi} \in \mathbb{R}^{m \times |\phi|}$ the set of the columns indexed by ϕ. Moreover, inspired by the analysis of the binary matrix-based compressed sensing (Donoho, 2006), in Definition 1 we model the adjacency relation between the binary matrix's rows and columns, which corresponds to the mapping relation between the coordinates of original data x and projected data x'. The relation will be explored in the following distance preservation analysis.

Definition 1 (Adjacency relation between the binary matrix's rows and columns)**.** Consider the binary matrix $R \in \{0, 1\}^{m \times n}$ with its columns and rows indexed by the variables j and i, respectively. For the matrix's j-th column, define its adjacent row set as $\mathcal{N}(j) = \{i : R_{i,j} \neq 0, i \in [m]\}$; and subsequently, for a

subset of the columns $J \subset [n]$, define its adjacent row set as $\mathcal{N}(J) = \{\bigcup_j N(j), j \in [J]\}$. Similarly, for the matrix's i-th row, define its adjacent column set as $\mathcal{N}(i) = \{j : R_{i,j} \neq 0, j \in [n]\}$. Notice that the matrix's columns and rows correspond respectively to the element coordinates of the original data x and projected data x', and so the adjacency relation defined above can be used to describe the mapping relation between the coordinates of the two kinds of data.

3.2 Original data

The analysis of the quantized random projection is related to the distribution of the original data $x = (x_1, x_2, \cdots, x_n)^\top \in \mathbb{R}^n$. In the paper, we propose to study the data with approximately sparse or exactly sparse distributions, as specified in Definitions 2 and 3.

Definition 2 (Approximately sparse data)**.** A data vector $x \in \mathbb{R}^n$ is called approximately sparse, if its element-magnitude-ordered version $x^* = (x_1^*, x_2^*, \cdots, x_n^*)$ follows an exponential decay relation: $|x_{i+1}^*|/|x_i^*| \leq e^{-\beta}$, where β is an arbitrary positive constant; and the larger the value of β, the faster the decaying speed.

Definition 3 (Exactly sparse data)**.** A data vector $x \in \mathbb{R}^n$ is called k sparse, or having sparsity k, if it contains exactly k ($\ll n$) nonzero entries, or say having the support size $|supp(x)| = k$, $supp(x) = \{i : x_i \neq 0, i \in [n]\}$.

The approximately sparse data are common in various classification tasks, such as the features extracted with DCT, DWT, CNN and so on. It is known that these features have approximately sparse distributions, and can be modeled with exponential decay functions (Weiss & Freeman, 2007; Kotz et al., 2012). Moreover, they can be further transformed to exactly sparse structures by zeroing out the elements of small magnitude. Compared to approximately sparse structures, exactly sparse structures have three advantages. First, it can help reduce the computation complexity of the downstream random projection operation. Second, as studied in (Lu et al., 2023), it tends to improve feature discrimination, favorable for classification. Third, as detailed latter, it is more easy to analyze, and allows us to simply set the projection's quantization threshold to be a constant value, zero. Therefore, in the final experiments we will pay more attention to the performance of exactly sparse features.

3.3 Quantization function

We adopt two simple yet popular quantization operations, the ternary and binary quantization. The ternary quantization is formulated as

$$f_\tau(x_i) = \begin{cases} +1, & x_i > \tau \\ -1, & x_i < -\tau \\ 0, & \text{others} \end{cases} \tag{2}$$

where the threshold parameter $\tau \geq 0$ will be empirically determined to control the sparsity of the quantization $f_\tau(x)$ of the vector $x \in \mathbb{R}^n$. Here we take $f_\tau(\cdot)$ as an element-wise function and write the vector's quantization $f_\tau(x) = (f_\tau(x_1), f_\tau(x_2), \cdots, f_\tau(x_n))^\top$. In a similar manner, the $\{0, 1\}$-binary quantization can be formulated using only one threshold parameter τ. For brevity, in the following we will focus our analysis on ternary quantization, and the analysis can be readily extended to binary quantization.

3.4 Distance preservation

Consider the random projection model (1), which has two original data u, $v \in \mathbb{R}^n$ and corresponding projections u', $v' \in \mathbb{R}^m$. We aim to determine the distribution of binary matrix R that ensures the following distance preservation property

$$f_{\tau_3}(u')^\top f_{\tau_4}(v') = \alpha \cdot f_{\tau_1}^\top(u) f_{\tau_2}(v) \tag{3}$$

holding with high probability, where α is a positive constant, and the threshold parameters τ_i of the quantization functions $f(\cdot)$ will be determined by analysis. Notice that for the convenience of analysis, the parameter α is introduced to define a relative distance preservation, whose value varying does not affect the classification of projected data; and the exact distance preservation, namely the case of $\alpha = 1$, can be easily obtained by scaling the element values of random matrix.

Different from the traditional quantized random projection model that requires preserving the distance between two original data u and v, our proposed distance preservation model (3) maintains the distance between the two original data's quantization codes, $f_{\tau_1}(u)$ and $f_{\tau_2}(v)$. This proposal is inspired by the recent finding (Lu et al., 2023) that the quantization of sparse features (i.e. our original data) can produce more discriminative features for classification. Then compared to the conventional distance preservation, the proposal (3) will help the projection to acquire more discriminative features from the original data. Also, the proposal can facilitate analysis, since the quantization operation on original data simplifies the data distribution.

4 Distance preservation analysis

For the projection matrix $R \in \{0,1\}^{m\times n}$ with varying column degree d, in this section we estimate the optimal column degree d that ensures the proposed distance preservation property (3) holding with high probability. For ease of analysis, we first describe the desired matrix structure that ensures the property (3) holding with two given data $x \in \mathbb{R}^n$, and then derive the probability that the desired matrix structure holds with two arbitrary data $x \in \mathbb{R}^n$. The analysis results are presented in Theorems 1-3, with comprehensive proofs outlined in Appendices A.1-A.3. For brevity, we mainly analyze the ternary quantized projections $f_\tau(x')$, and the analysis can be straightforwardly extended to the binary case.

4.1 Distance preservation for two given data

Given two original data points u, $v \in \mathbb{R}^n$ with deterministic structures, we evaluate the distance preservation condition separately in Theorems 1 and 2 for two typical data distributions: exactly sparse and approximately sparse, as specified in Definitions 3 and 2. On the whole, both theorems demonstrate that the proposed distance preservation (3) will be achieved, if the submatrix $R_{*,\phi}$ of the binary matrix R, indexed by the support union ϕ of the two quantization codes $f_{\tau_1}(u)$ and $f_{\tau_2}(v)$ corresponding to the two original data points, has orthogonal columns. The details are discussed in their respective remarks.

Theorem 1 (Exactly sparse data)**.** Consider the random projection model (1), which has two projected data u', $v' \in \mathbb{R}^m$ generated from two exactly sparse data u, $v \in \mathbb{R}^n$ with sparsity k_1, k_2, provided a random matrix $R \in \{0,1\}^{m\times n}$ with column degree d ($< m$). Let $\phi = supp(u) \cup supp(v)$, then $|\phi| \le k_1 + k_2$. If $R_{*,\phi}^\top R_{*,\phi} = dI_{|\phi|}$, where $I_{|\phi|}$ denotes the identity matrix of size $|\phi|$, we have

$$f_0(u')^\top f_0(v') = d \cdot f_0(u)^\top f_0(v), \tag{4}$$

where $f_0(\cdot)$ is the ternary quantization function (2) with parameter $\tau = 0$.

Remark of Theorem 1. For the theorem, there are three issues worth stating. (i) It is easy to see that the orthogonal $R_{*,\phi}$ required by the theorem could be obtained, if the size of the support union of two original data is less than the matrix's row size, that is $|\phi| \le m$. This condition can be easily achieved by zeroing out the small-magnitude elements of sparse features, and as stated before, this sparsifying operation can improve feature discrimination, beneficial to classification (Lu et al., 2023). (ii) The four ternary functions of (4) all simply fix their threshold parameter to be $\tau = 0$ for both the original data and projected data, avoiding the burden of parameter tuning. (iii) The derivation of (4) depends on the distribution of the nonzero entries of binary matrix, but not on their specific values. Therefore, the result (4) is also available for the random $\{0, \pm 1\}$-ternary matrix. In the paper, we will focus on binary matrices for its simpler structure. (iv) The ternary or binary quantization of exactly sparse data remains exactly sparse, and the quantization can be used for easier projection, without altering the final projection result (4). In other words, Theorem 1 holds for the random projection model which has both the original data and projected data quantized to be ternary or binary codes.

Theorem 2 (Approximately sparse data)**.** Consider the random projection model (1), which has two projected data u', $v' \in \mathbb{R}^m$ generated from two approximately sparse data u, $v \in \mathbb{R}^n$, provided a random matrix $R \in \{0,1\}^{m\times n}$ with column degree d. For u and v, assigning two ternary functions $f_\tau(\cdot)$ with $\tau = \tau_1 = \frac{|u^*_{k_1}|+|u^*_{k_1+1}|}{2}$ and $\tau = \tau_2 = \frac{|v^*_{k_2}|+|v^*_{k_2+1}|}{2}$, respectively, such that $supp(f_{\tau_1}(u)) = k_1$ and

$supp(f_{\tau_2}(v)) = k_2$, where $u^*_{k_1}$ denotes the k_1-th largest element of u in magnitude and $v^*_{k_2}$ is defined similarly. Let $\phi = supp\,(f_{\tau_1}(u)) \cup supp(f_{\tau_2}(v))$, then $|\phi| \leq k_1 + k_2$. If $R^\top_{*,\phi} R_{*,\phi} = dI_{|\phi|}$ and u, v have their decaying parameter $\beta \geq \ln(2+\sqrt{3})$, we can derive that

$$f_{\tau_1}(u')^\top f_{\tau_2}(v') = d \cdot f_{\tau_1}(u)^\top f_{\tau_2}(v). \tag{5}$$

Remark of Theorem 2. (i) The analysis and result for approximately sparse data are similar to those we have obtained for exactly sparse data in Theorem 1. One of major differences is the choice of the threshold parameter τ for ternary functions. As discussed in Section 3.4, we need to select a proper τ to produce a data sparsity k that can improve feature discrimination when transforming u to $f_\tau(u)$, thus leading to better classification performance. As shown in (Lu et al., 2023), the desired sparsity k can be empirically determined. Without loss of generality, we assume two different sparsity values k_1, k_2 (corresponding to τ_1 and τ_2) for the two original data points u, v, in order to obtain the desired quantization performance. In practical applications, for simplicity, we suggest to select a same sparsity k for the two data, since they are generally obtained from the same scene and share similar distributions. (ii) Moreover, it is worth noting that besides the orthogonal constraint on the submatrix $R_{*,\phi}$, the derivation of (5) also imposes a constraint on the distribution of the original sparse data: the data should have its decaying parameter $\beta \geq \ln(2+\sqrt{3})$, and roughly speaking, the data needs to decay sufficiently fast. Notice that the lower bound for β is a sufficient but not necessary condition, and empirically our optimal matrix estimation is not sensitive to the lower bound of β and tends to achieve the desired classification performance even for the sparse features with smaller β.

4.2 Distance preservation for two arbitrary data

To generalize the distance preservation property (3) from two fixed data to arbitrary data, we should extend the condition of orthogonal $R_{*,\phi}$ from a fixed column set $\phi = supp\,(f_{\tau_1}(u)) \cup supp(f_{\tau_2}(v))$ to an arbitrary set $\phi \subset [n]$, $|\phi| = k_1 + k_2 < m$. For a randomly generated binary matrix $R \in \{0,1\}^{m\times n}$, however, it is hard to ensure its each submatrix $R_{*,\phi}$ to have orthogonal columns. In Theorem 3, we analyze the probability of having orthogonal $R_{*,\phi}$ under the varying column degree d.

Theorem 3. Given a random matrix $R \in \{0,1\}^{m\times n}$ with column degree d. Consider its submatrix $R_{*,\phi}$ with $\phi \subset [n]$. Denote $Pr\{R^\top_{*,\phi} R_{*,\phi} = dI_{|\phi|}\}$ as the probability of $R^\top_{*,\phi} R_{*,\phi} = dI_{|\phi|}$ holding for any $\phi \subset [n]$, with $|\phi| \geq 2$ and $d|\phi| \leq m$. Provided m and ϕ, we have the probability

$$Pr\{R^\top_{*,\phi} R_{*,\phi} = dI_{|\phi|}\} = \frac{[(m-d)!]^{|\phi|}}{(m!)^{(|\phi|-1)}(m-|\phi|d)!} \tag{6}$$

$$\leq \frac{\prod_{\ell=1}^{|\phi|-1}(m-\ell)}{m^{|\phi|-1}} \tag{7}$$

which has the value of (6) monotonically decreasing with the column degree d, and has the equality of (7) achieved by $d = 1$.

Remark of Theorem 3. (i) The theorem demonstrates that the probability (6) of having orthogonal $R_{*,\phi}$ will increase with the decreasing of column degree d. It suggests that the distance preservation property (3) should be satisfied with higher probability by the binary matrix with smaller column degree d. Then it is reasonable to conjecture that when applied to the common classification or clustering tasks, quantized projections can achieve the best performance with very sparse binary matrices, i.e. the ones with column degree as small as $d = 1$, as verified in our experiments. (ii) Moreover, it is worth noting that besides the column degree d, the probability (6) is also related to the size of ϕ. For the probability derived with $d = 1$ in (7), it is easy to see that the smaller the $|\phi|$, the higher the probability. This means that the more sparse features x (with smaller sparsity k) should result in the better distance preservation property (3), and this relation is similar to the condition of compressed sensing (Donoho, 2006).

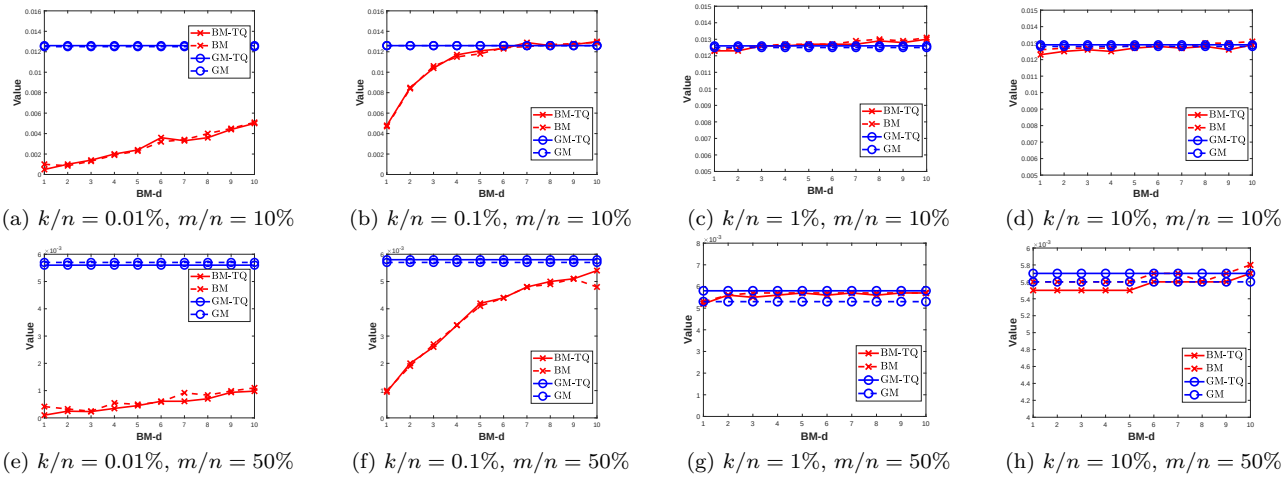

(a) $k/n = 0.01\%$, $m/n = 10\%$ (b) $k/n = 0.1\%$, $m/n = 10\%$ (c) $k/n = 1\%$, $m/n = 10\%$ (d) $k/n = 10\%$, $m/n = 10\%$

(e) $k/n = 0.01\%$, $m/n = 50\%$ (f) $k/n = 0.1\%$, $m/n = 50\%$ (g) $k/n = 1\%$, $m/n = 50\%$ (h) $k/n = 10\%$, $m/n = 50\%$

Figure 1: Distance variation rate for the ternary-quantized (TQ) (and non-quantized) projections of the generated data, with four different feature sparsity ratios $k/n = 0.01\%$, 0.1%, 1% and 10%, using two projection matrices: the Gaussian matrix (GM) and the binary matrix (BM) with varying column degree BM-d $\in [1, 10]$, under two projection ratios $m/n = 10\%$ and 50%. Note the smaller the distance variation rate, the better the distance preservation.

4.3 Extension to binary quantization

In Theorems 1 and 2, we only investigate the ternary quantization (2) for the distance preservation condition (3). From the proofs of the two theorems, it can be seen that their results can be directly extended to the case of binary quantization, with the same threshold values τ_i. Then by Theorem 3, we can predict that the binary quantization of projected data will achieve its best classification performance when using very sparse binary matrices. This is verified in our experiments. In the paper, we pay more attention to ternary quantization than to binary quantization, as the latter generally performs worse due to discarding more feature elements (Lu et al., 2023).

4.4 Numerical analysis

In this part, we aim to validate the main result of Theorem 3, namely the proposed distance preservation property (3) should be held with higher probability by binary matrices with smaller column degrees d, when the sparsity ratio k/n of the quantization $f_{\tau_i}(\cdot)$ of original data is sufficiently small, as required in Theorems 1 and 2. For this purpose, we directly investigate the distance varying by numerical simulations. By the distance preservation property (3), we define the *distance variation rate* of the pairwise distance between the quantized projected data, relative to the distance between the quantized original data using the formula

$$\frac{1}{N}\sum_{i=1}^{N}\frac{\left|\|f_{\tau_3}(u^{(i)\prime}) - f_{\tau_4}(v^{(i)\prime})\|_2 - \|f_{\tau_1}(u^{(i)}) - f_{\tau_2}(v^{(i)})\|_2\right|}{\|f_{\tau_1}(u^{(i)}) - f_{\tau_2}(v^{(i)})\|_2} \tag{8}$$

where $u^{(i)}$, $v^{(i)} \in \mathbb{R}^n$ are a pair of original data points, $1 \le i \le N$, and $u^{(i)\prime}$, $v^{(i)\prime} \in \mathbb{R}^m$ are their projections over a random matrix $R \in \{0, 1\}^{m\times n}$ with column degree d. Note that all the quantized data $f_{\tau_i}(\cdot)$ in (8) are pre-normalized using ℓ_2 norm, in order to eliminate the magnitude discrepancy between before and after random projections. It is evident that the smaller the distance variation rate (8), the better the distance preservation property.

To flexibly control the sparsity ratio k/n of the quantization $f_{\tau_i}(\cdot)$ of original data, we simply set $\tau = 0$ and randomly generate the original data $u^{(i)}$, $v^{(i)}$ by controlling the number k of nonzero entries. By Theorems 1 and 2, the specific values of the nonzero entries will not affect the distance preservation property. For ease of simulation, we set $u^{(i)}$, $v^{(i)} \in \{0, \pm 1\}^n$ for the study of ternary quantization. Moreover, we set the number of data pairs $N = 10000$, the original data dimension $n = 10000$, the data sparsity ratio $k/n \in \{0.01\%, 0.1\%, 1\%, 10\%\}$, the binary matrices' column degree $d \in [1, 10]$, and the projection ratio $m/n \in \{10\%, 50\%\}$.

The simulation results are provided in Figure 1. For comparison, the results for the popular Gaussian matrix-based random projection are also provided. Figure 1 illustrates that as expected in Theorem 3, the distance variation rate of random binary matrices inclines to increase with the column degree d. This indicates a decline in distance preservation capability. This trend is particularly evident, when the sparsity ratio k/n of original data is relatively small, such as $k/n < 1\%$. This is consistent with our theoretical analysis. As the sparsity ratio k/n increases, binary matrices tend to exhibit similar distance preservation performance across different column degrees d. Compared to Gaussian matrices, binary matrices can often achieve lower distance variation rates, indicating better distance preservation performance, especially for small values of k/n. As k/n increases, two kinds of matrices tend to exhibit comparable distance preservation performance. These trends are also observed in the case of binary quantization, where both the original and projected data are quantized to $\{0, 1\}$-binary values, as detailed in Appendix A.4.1, Figure 7. Notably, the above performance trends regarding distance preservation are corroborated in subsequent experiments on classification and clustering, providing further validation of our theoretical insights.

5 Experiments

5.1 Setting

In this section, we investigate the performance of the ternary and binary-quantized projections of sparse data in both supervised and unsupervised learning tasks, specifically classification and clustering. Random projections are implemented using random binary matrices with different column degrees. Our goal is to find the column degree that leads to the best classification or clustering performance. For comparison, the performance is also tested for the popular Gaussian matrix-based random projections and for the non-quantized projections. Considering both the ternary and binary-quantized projections commonly exhibit similar performance trends with the varying of the column degree of binary matrices, we will mainly discuss the results of ternary projections and defer the results of binary projections to Appendix A.4.

5.1.1 Classification and clustering algorithms

To directly reflect the impact of the distance between projected data on classification and clustering, we employ linear similarity metrics-based algorithms for both tasks. Specifically, classification is implemented with two typical linear classifiers, the K-nearest neighbor (KNN) classifier with cosine distance (Peterson, 2009) and the support vector machines (SVM) with linear kernel (Cortes & Vapnik, 1995). Both classifiers have performance fully dependent on the distance between data, without involving additional operations to further improve data discrimination. Empirically, the two classifiers tend to show similar performance trends as the column degree of binary matrices varies. For brevity, we will focus on the results of KNN and present the results of SVM (Cortes & Vapnik, 1995) in Appendix A.4. Clustering is realized with the k-means algorithm with cosine distance (MacQueen et al., 1967). To evaluate clustering accuracy, we follow the strategy adopted in (Xu et al., 2004). Given a set of labeled data, we first remove their labels to run the clustering algorithm, then label each resulting cluster with the majority class according to the original data labels, and calculate the proportion of the data samples correctly classified by each cluster.

5.1.2 Data

The sparse data to be projected are generated from the datasets YaleB (Georghiades et al., 2001; Lee et al., 2005), CIFAR10 (Krizhevsky & Hinton, 2009) and Mini-ImageNet (Vinyals et al., 2016), respectively via the feature transforms DWT (Mallat, 2009), AlexNet Conv5 (Krizhevsky et al., 2012) and VGG16 Conv5_3 (Simonyan & Zisserman, 2014). To provide relatively good classification performance, we assign more advanced feature transforms to more complex datasets. The datasets are briefly introduced as follows. YaleB contains the face images of 38 persons, with about 64 samples per person. From the dataset, we randomly select 9/10 samples for training and the rest for testing. CIFAR10 consists of 10 classes of color images, with 6000 samples per class. Mini-ImageNet is a subset of ImageNet (Deng et al., 2009), which consists of 100 classes of color images, each class having 600 samples. For the latter two datasets, we use their default training and testing samples, with the ratio of 5/1. For the three datasets, we normalize the

feature vectors with zero mean and unit variance, and reduce the vector dimensions several times to the order of thousands for easier simulation. The dimension reduction may decrease the classification or clustering accuracy but not influence our comparative study. To verify Theorems 1 and 2, we evaluate two kinds of sparse data that have approximately and exactly sparse distributions, respectively, as specified in Definitions 2 and 3. The approximately sparse ones are the original sparse features generated with DWT and CNN, and the exactly sparse ones are obtained by further sparsifying the features with given sparsity ratios of $k/n = 1\%$, 5%, 10% and 20%. Compared to the original, approximately sparse features, as mentioned earlier, the resulting exactly sparse features are usually more favorable for classification (Lu et al., 2023). For the random projection model (1), we test two different projection ratios: $m/n = 10\%$ and 50%.

5.2 Classification results

The classification results are provided in Figures 2-5 and Figure 6, respectively for the exactly sparse features and the approximately sparse features. In each figure, the first and second rows correspond respectively to the random projection cases of projection ratios $m/n = 10\%$ and 50%, and the four subfigures in each row correspond to the exactly sparse features with sparsity ratio $k/n = 1\%$, 5%, 10% and 20%. Considering the fact that exactly sparse features outperform approximately sparse features, and ternary quantization outperforms binary quantization (Lu et al., 2023), for brevity, we mainly analyze the classification on the ternary quantized projections of exactly sparse features, as illustrated in Figures 2-4. The analysis is conducted from the following several aspects.

5.2.1 Binary matrices with different column degrees

By the remark of Theorem 3, the proposed distance preservation property (3) tends to be held with higher probability, when the binary matrix has a smaller column degree d. Then, the classification accuracy of quantized projections is expected to decrease with the increased column degree d. This performance trend is basically verified by the results illustrated in Figures 2-4, see the x-marked, solid lines for the classification of the ternary quantized projections of the exactly sparse features with different sparsity ratios $k/n = 1\%$, 5%, 10% and 20%. It can be seen that the performance declining speed differs with different data types, and it seems that the more easy the data for classification, such as the DWT features of YaleB shown in Figure 2, the more obvious the performance advantage of $d = 1$ over other larger d. An exception worth mentioning is the case of $k/n = 1\%$, as shown in Figures 2 and 3, where $d = 1$ performs slightly worse than $d = 2$. This deviation should be attributed to the gap between theory and practice: the classification of quantized projections relates not only to the distance preservation property studied here, but also to other factors out of our scope, such as feature discrimination. Despite the imperfect, our theoretical estimation is generally supported by the results of Figures 2-4: the column degree $d = 1$ tends to provide better or at least comparable performance to other larger d, in the classification of the ternary-quantized projections of exactly sparse features.

5.2.2 Quantized vs. non-quantized projections

By (Lu et al., 2023), quantized projections can provide better classification performance than non-quantized projections, if both the original data and random matrix have sufficiently sparse distributions, and the quantization threshold τ for projected data is properly selected. This performance property is also proved in our experiments. Comparing the classification results provided in Figures 2-4 for the ternary-quantized projections (x-marked, solid lines) and non-quantized projections (x-marked, dashed lines), it can be seen that the former tends to achieve better performance than the latter, when the column degree d of binary matrix and the sparsity ratio k/n of original data (i.e. the exactly sparse features) both become smaller, such as the case of d=1 and $k/n = 1\%$. Note that by Theorem 1 we here simply set the quantization threshold as $\tau = 0$, and the better performance for quantized projections should be obtained if the threshold is more carefully selected as in (Lu et al., 2023). Overall, the above results indicate that the sparse binary matrix with $d = 1$ can obtain better classification performance on quantized projections than on non-quantized projections. This result is highly attractive both in terms of complexity and accuracy.

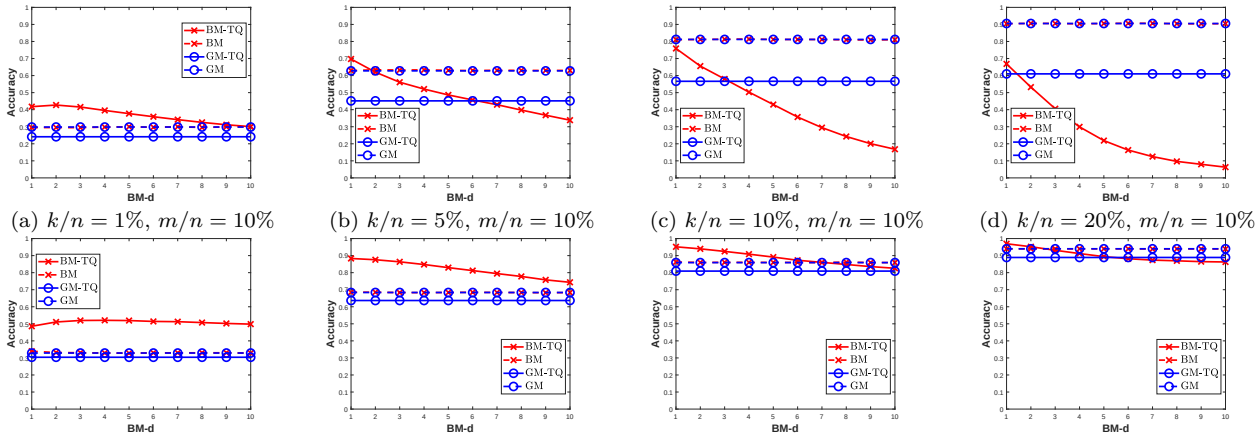

(a) $k/n = 1\%$, $m/n = 10\%$ (b) $k/n = 5\%$, $m/n = 10\%$ (c) $k/n = 10\%$, $m/n = 10\%$ (d) $k/n = 20\%$, $m/n = 10\%$

(e) $k/n = 1\%$, $m/n = 50\%$ (f) $k/n = 5\%$, $m/n = 50\%$ (g) $k/n = 10\%$, $m/n = 50\%$ (h) $k/n = 20\%$, $m/n = 50\%$

Figure 2: Classification accuracy for the ternary-quantized (TQ) (and non-quantized) projections of the exactly sparse features of YaleB (DWT), with three different feature sparsity ratios $k/n = 1\%$, 5%, 10% and 20%, using two projection matrices: the Gaussian matrix (GM) and the binary matrix (BM) with varying column degree BM-d $\in [1, 10]$, under two projection ratios $m/n = 10\%$ and 50%.

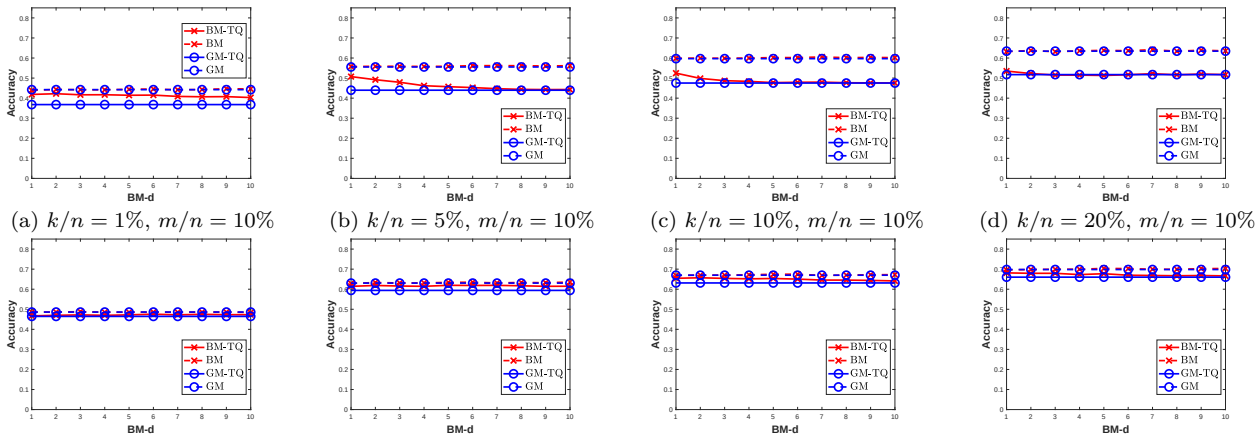

(a) $k/n = 1\%$, $m/n = 10\%$ (b) $k/n = 5\%$, $m/n = 10\%$ (c) $k/n = 10\%$, $m/n = 10\%$ (d) $k/n = 20\%$, $m/n = 10\%$

(e) $k/n = 1\%$, $m/n = 50\%$ (f) $k/n = 5\%$, $m/n = 50\%$ (g) $k/n = 10\%$, $m/n = 50\%$ (h) $k/n = 20\%$, $m/n = 50\%$

Figure 3: Classification accuracy for the ternary-quantized (TQ) (and non-quantized) projections of the exactly sparse features of CIFAR10 (AlexNet), with three different feature sparsity ratios $k/n = 1\%$, 5%, 10% and 20%, using two projection matrices: the Gaussian matrix (GM) and the binary matrix (BM) with varying column degree BM-d $\in [1, 10]$, under two projection ratios $m/n = 10\%$ and 50%.

5.2.3 Binary matrices vs. Gaussian matrices

Figures 2-4 demonstrate that binary matrices (x-marked solid lines) tend to outperform Gaussian matrices (circle-marked solid lines), as the column degree d of binary matrix and the sparsity ratio k/n of original data both become smaller, such as the case of d=1 and $k/n = 1\%$. The superior performance of binary matrices should be attributed to its advantage in distance preservation, as demonstrated in Section 4.4. In this case, we are encouraged to replace Gaussian matrices with sparse binary matrices, for improvements both in complexity and accuracy.

5.2.4 Binary quantized projections

By the discussion in Section 4.3, the theoretical properties of binary matrices we derive with ternary quantized projections in Theorems 1-3 should also hold with binary quantized projections. In other words, the performance trends derived in Figures 2-4 for ternary projections, should be also achievable for binary projections. To verify this, we examine the classification on binary projections in Figure 5, see Appendix A.4.2

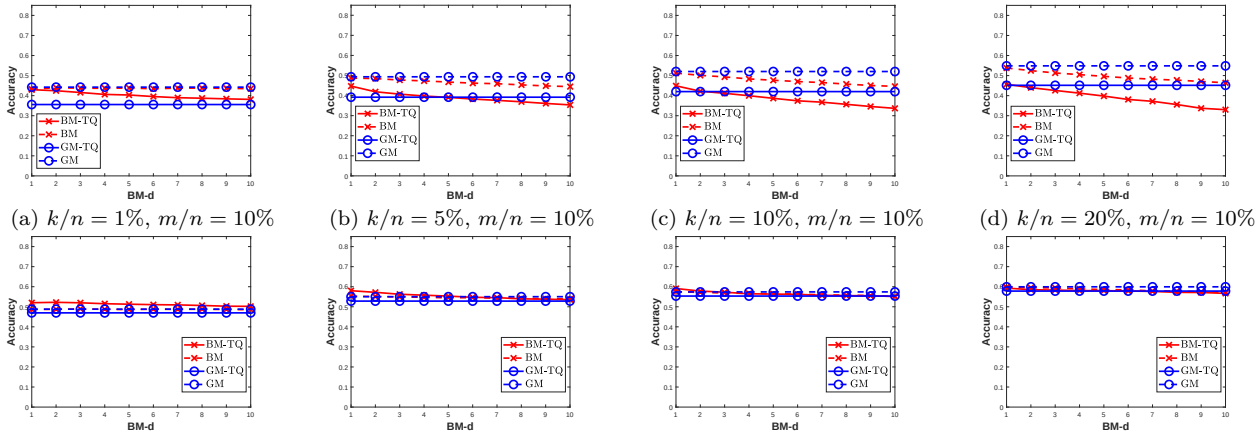

(a) $k/n = 1\%$, $m/n = 10\%$ (b) $k/n = 5\%$, $m/n = 10\%$ (c) $k/n = 10\%$, $m/n = 10\%$ (d) $k/n = 20\%$, $m/n = 10\%$

(e) $k/n = 1\%$, $m/n = 50\%$ (f) $k/n = 5\%$, $m/n = 50\%$ (g) $k/n = 10\%$, $m/n = 50\%$ (h) $k/n = 20\%$, $m/n = 50\%$

Figure 4: Classification accuracy for the ternary-quantized (TQ) (and non-quantized) projections of the exactly sparse features of Mini-ImageNet (VGG16), with three different feature sparsity ratios $k/n = 1\%$, 5%, 10% and 20%, using two projection matrices: the Gaussian matrix (GM) and the binary matrix (BM) with varying column degree BM-d $\in [1, 10]$, under two projection ratios $m/n = 10\%$ and 50%.

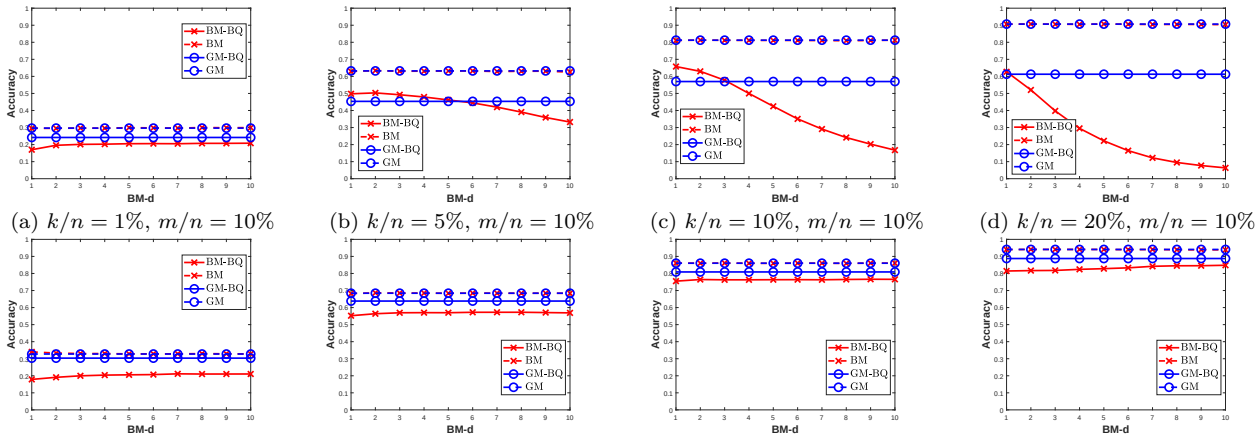

(a) $k/n = 1\%$, $m/n = 10\%$ (b) $k/n = 5\%$, $m/n = 10\%$ (c) $k/n = 10\%$, $m/n = 10\%$ (d) $k/n = 20\%$, $m/n = 10\%$

(e) $k/n = 1\%$, $m/n = 50\%$ (f) $k/n = 5\%$, $m/n = 50\%$ (g) $k/n = 10\%$, $m/n = 50\%$ (h) $k/n = 20\%$, $m/n = 50\%$

Figure 5: Classification accuracy for the binary-quantized (BQ) (and non-quantized) projections of the exactly sparse features of YaleB (DWT), with three different feature sparsity ratios $k/n = 1\%$, 5%, 10% and 20%, using two projection matrices: the Gaussian matrix and the binary matrix with varying column degree BM-d $\in [1, 10]$, under two projection ratios $m/n = 10\%$ and 50%.

for more results. Figure 5 shows that similarly as the classification of ternary projections, in the classification of binary projections the binary matrix with column degree $d = 1$ exhibits better or at least comparable performance than other more dense counterparts. Moreover, it is worth mentioning that binary quantization performs worse than ternary quantization, as found in (Lu et al., 2023), due to discarding more feature elements.

5.2.5 Approximately sparse features

In Figure 6, we provide the classification results on the ternary quantized projections of the original features, which have approximately sparse structures. As theoretically expected, binary matrices with $d = 1$ achieve better or at least comparable performance to other denser matrices. Empirically, these approximately sparse features do not precisely meet the decay speed β required in Theorem 2. This implies that our theoretical findings exhibit robust universal applicability, being relatively insensitive to the sparsity conditions imposed on the original data. With the increasing of k/n, as illustrated in Figures 2-6, the performance advantage of

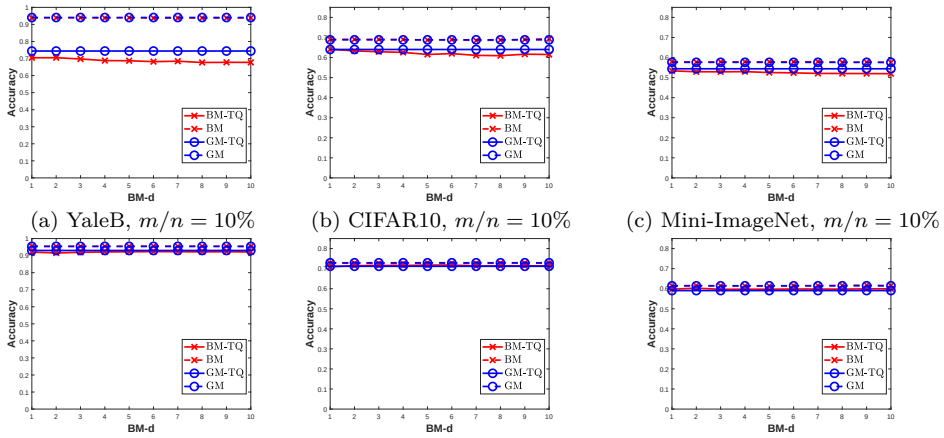

(a) YaleB, $m/n = 10\%$ (b) CIFAR10, $m/n = 10\%$ (c) Mini-ImageNet, $m/n = 10\%$

(d) YaleB, $m/n = 50\%$ (e) CIFAR10, $m/n = 50\%$ (f) Mini-ImageNet, $m/n = 50\%$

Figure 6: Classification accuracy for the ternary-quantized (TQ) (and non-quantized) projections of the original, approximately sparse features: YaleB (DWT), CIFAR10 (AlexNet), Mini-ImageNet (VGG16), using two projection matrices: the Gaussian matrix (GM) and the binary matrix (BM) with varying column degree BM-d $\in [1, 10]$, under two projection ratios $m/n = 10\%$ and 50%.

binary matrices over Gaussian matrices will become less evident in the classification of quantized projections. This performance trend is consistent with the distance preservation property illustrated in Figure 1. Finally, recall that the original, approximately sparse features tend to achieve higher classification accuracy, if being further simplified to exactly sparse structures (Lu et al., 2023). Then for both better classification and easier computation, we are motivated to transform theses features to exactly sparse structures before conducting random projections on them.

5.3 Clustering results

For limited space, we provide the clustering results on the *ternary* and *binary* quantized projections in Appendix A.4.3, specifically depicted in Figures 11-13 and Figures 14-16, respectively. Similarly as in classification, the extremely sparse binary matrix with column degree $d = 1$ exhibits several similar properties in clustering: 1) it can achieve superior or comparable performance to other denser binary matrices with larger d values, as well as Gaussian matrices; 2) its performance on quantized projections is often better than on non-quantized projections. 3) these performance advantages can endure even when the feature sparsity ratio k/n increases from 1% to 20%, gradually deviating from the theoretical condition on feature sparsity.

6 Conclusion

For the binary matrix-based random projection, where the projections are further quantized to binary or ternary values, we have investigated how the sparsity of binary matrices influences the ability of the quantized projections to preserve pairwise distances between the quantized original data. Our analysis indicates that binary matrices with sparser structures tend to better maintain pairwise distances, particularly when the original data intended for projections exhibit sufficiently sparse structures. This performance trend has been corroborated in classification and clustering experiments conducted on quantized projections of common data features, such as the DWT of YaleB and the CNN of CIFAR10 and ImageNet, all of which exhibit approximately sparse structures. In these experiments, extremely sparse binary matrices with only one nonzero entry per column generally provide better or comparable classification performance compared to denser binary matrices and Gaussian matrices. The extremely sparse matrix structure significantly reduces the complexity of the quantized random projection models, such as the large-scale retrieval model (Charikar, 2002). Furthermore, our research offers insights into the sparse structures inherent in other advanced models that incorporate quantized projection architectures, like deep quantization networks (Wan et al., 2018; Qin et al., 2020), as well as biological neuron models (Dasgupta et al., 2017).

References

D. Achlioptas. Database-friendly random projections: Johnson–Lindenstrauss with binary coins. *J. Comput. Syst. Sci.*, 66(4):671–687, 2003.

Petros T Boufounos and Shantanu Rane. Efficient coding of signal distances using universal quantized embeddings. In *Data Compression Conference*, pp. 251–260, 2013.

Moses S Charikar. Similarity estimation techniques from rounding algorithms. In *Proceedings of the thiry-fourth annual ACM symposium on Theory of computing*, pp. 380–388, 2002.

Corinna Cortes and Vladimir Vapnik. Support-vector networks. *Machine learning*, 20(3):273–297, 1995.

S. Dasgupta and A. Gupta. An elementary proof of the Johnson–Lindenstrauss lemma. *Technical Report, UC Berkeley*, (99–006), 1999.

Sanjoy Dasgupta, Charles F Stevens, and Saket Navlakha. A neural algorithm for a fundamental computing problem. *Science*, 358(6364):793–796, 2017.

J. Deng, W. Dong, R. Socher, L.-J. Li, K. Li, and L. Fei-Fei. ImageNet: A Large-Scale Hierarchical Image Database. In *IEEE Conference on Computer Vision and Pattern Recognition*, 2009.

D.L. Donoho. Compressed sensing. *IEEE Transactions on Information Theory*, 52(4):1289–1306, 2006.

Thierry Eude, Richard Grisel, Hocine Cherifi, and Roland Debrie. On the distribution of the dct coefficients. In *IEEE International Conference on Acoustics, Speech and Signal Processing*, pp. V–365. IEEE, 1994.

A. Georghiades, P. Belhumeur, and D. Kriegman. From few to many: Illumination cone models for face recognition under variable lighting and pose. *IEEE Trans. PAMI*, 23(6):643–660, 2001.

Arvind Iyer and Johannes Burge. The statistics of how natural images drive the responses of neurons. *Journal of vision*, 19(13):4–4, 2019.

Laurent Jacques, Jason N Laska, Petros T Boufounos, and Richard G Baraniuk. Robust 1-bit compressive sensing via binary stable embeddings of sparse vectors. *IEEE Transactions on Information Theory*, 59(4): 2082–2102, 2013.

W. B. Johnson and J. Lindenstrauss. Extensions of Lipschitz mappings into a Hilbert space. *Contemp. Math.*, 26:189–206, 1984.

Samuel Kotz, Tomasz Kozubowski, and Krzystof Podgorski. *The Laplace distribution and generalizations: a revisit with applications to communications, economics, engineering, and finance*. Springer Science & Business Media, 2012.

A. Krizhevsky and G. Hinton. Learning multiple layers of features from tiny images. *Master's thesis, Department of Computer Science, University of Toronto*, 2009.

Alex Krizhevsky, Ilya Sutskever, and Geoffrey E Hinton. Imagenet classification with deep convolutional neural networks. In *Advances in Neural Information Processing Systems*, 2012.

K. Lee, J. Ho, and D. Kriegman. Acquiring linear subspaces for face recognition under variable lighting. *IEEE Trans. PAMI*, 27(5):684–698, 2005.

P. Li, T. J. Hastie, and K. W. Church. Very sparse random projections. *in Proceedings of the 12th ACM SIGKDD international conference on Knowledge discovery and data mining*, 2006.

Ping Li, Michael Mitzenmacher, and Anshumali Shrivastava. Coding for random projections. In *International Conference on Machine Learning*, pp. 676–684. PMLR, 2014.

Wen-Ye Li and Shu-Zhong Zhang. Binary random projections with controllable sparsity patterns. *Journal of the Operations Research Society of China*, 10(3):507–528, 2022.

Weizhi Lu, Weiyu Li, Wei Zhang, and Shu-Tao Xia. Expander recovery performance of bipartite graphs with girth greater than 4. *IEEE Transactions on Signal and Information Processing over Networks*, 5(3): 418–427, 2018.

Weizhi Lu, Mingrui Chen, Kai Guo, and Weiyu Li. Quantization: Is it possible to improve classification? In *Data Compression Conference*, pp. 318–327. IEEE, 2023.

James MacQueen et al. Some methods for classification and analysis of multivariate observations. In *Proceedings of the fifth Berkeley symposium on mathematical statistics and probability*, volume 1, pp. 281–297. Oakland, CA, USA, 1967.

Stphane Mallat. *A Wavelet Tour of Signal Processing, Third Edition: The Sparse Way*. Academic Press, Inc., Orlando, FL, USA, 3rd edition, 2009.

Rodrigo Mendoza-Smith and Jared Tanner. Expander ℓ_0-decoding. *Applied and Computational Harmonic Analysis*, March 2017. ISSN 1063-5203.

Leif E Peterson. K-nearest neighbor. *Scholarpedia*, 4(2):1883, 2009.

Haotong Qin, Ruihao Gong, Xianglong Liu, Xiao Bai, Jingkuan Song, and Nicu Sebe. Binary neural networks: A survey. *Pattern Recognition*, 105:107281, 2020.

K Ramamohan Rao and Ping Yip. *Discrete cosine transform: algorithms, advantages, applications*. Academic press, 2014.

Daniel L Ruderman. The statistics of natural images. *Network: computation in neural systems*, 5(4):517–548, 1994.

Eero P Simoncelli. Modeling the joint statistics of images in the wavelet domain. In *Wavelet Applications in Signal and Image Processing VII*, volume 3813, pp. 188–195. International Society for Optics and Photonics, 1999.

Karen Simonyan and Andrew Zisserman. Very deep convolutional networks for large-scale image recognition. *arXiv preprint arXiv:1409.1556*, 2014.

Diego Valsesia and Enrico Magli. Binary adaptive embeddings from order statistics of random projections. *IEEE Signal Processing Letters*, 24(1):111–115, 2016.

Oriol Vinyals, Charles Blundell, Timothy Lillicrap, Daan Wierstra, et al. Matching networks for one shot learning. *Advances in neural information processing systems*, 29, 2016.

Diwen Wan, Fumin Shen, Li Liu, Fan Zhu, Jie Qin, Ling Shao, and Heng Tao Shen. TBN: Convolutional neural network with ternary inputs and binary weights. In *Proceedings of the European Conference on Computer Vision*, pp. 315–332, 2018.

Yair Weiss and William T Freeman. What makes a good model of natural images? In *2007 IEEE Conference on Computer Vision and Pattern Recognition*, pp. 1–8. IEEE, 2007.

Linli Xu, James Neufeld, Bryce Larson, and Dale Schuurmans. Maximum margin clustering. In L. Saul, Y. Weiss, and L. Bottou (eds.), *Advances in Neural Information Processing Systems*, volume 17. MIT Press, 2004.

John Zarka, Louis Thiry, Tomas Angles, and Stephane Mallat. Deep network classification by scattering and homotopy dictionary learning. In *International Conference on Learning Representations*, 2020.

A Appendices

A.1 Proof of Theorem 1

Proof. For the two exactly sparse data points u, $v \in \mathbb{R}^n$, suppose their support intersection $\psi = supp(u) \cap supp(v)$. Then we can write

$$f_0(u)^\top f_0(v) = \sum_{j \in \psi} f_0(u_j) f_0(v_j). \tag{9}$$

Recall that $f_0(\cdot)$ is an element-wise function. Similarly, for the two projected points u', $v' \in \mathbb{R}^m$, we define their support union and intersection as $\phi' = supp(u') \cup supp(v')$ and $\psi' = supp(u') \cap supp(v')$, and then can write

$$f_0(u')^\top f_0(v') = \sum_{i \in \psi'} f_0(u'_i) f_0(v'_i). \tag{10}$$

In the sequel, we aim to prove that (10) can be linearly transformed to (9). The analysis of (10) requires us to first determine the support intersection ψ' between projected data. To achieve this, we examine the value of each element $f_0(u'_i)$ of $f_0(u')$, which for ease of analysis is divided into two groups on the basis of $i \in \mathcal{N}(supp(u))$ or not. Notice that the analysis will require us to frequently explore the adjacency relation between the random matrix's columns and rows, or say the mapping relation between the original data and projected data, as specified in Definition 1. For the case of $i \notin \mathcal{N}(supp(u))$, by Definition 1 we have $R_{i,j} = 0$, $\forall j \in supp(u)$, and then can write

$$\begin{aligned} f_0(u'_i) &= f_0\left(\sum_{j \in [n] \setminus supp(u)} R_{i,j} u_j\right) \\ &= 0 \end{aligned} \tag{11}$$

since $u_j = 0$, $\forall j \in [n] \setminus supp(u)$; otherwise, we can derive

$$\begin{aligned} f_0(u'_i) &\overset{1}{=} f_0\left(\sum_{j \in supp(u)} R_{i,j} u_j\right) \\ &\overset{2}{=} f_0\left(\sum_{j \in supp(u) \cap \mathcal{N}(i)} R_{i,j} u_j\right) \\ &\overset{3}{=} f_0\left(u_{j = supp(u) \cap \mathcal{N}(i)}\right) \\ &\overset{4}{\neq} 0 \end{aligned} \tag{12}$$

for the case of $i \in \mathcal{N}(supp(u))$. The derivation of (12) is detailed as follows: (i) The first equation results from the definition of $supp(u)$, which holds $u_i \neq 0$ for $i \in supp(u)$, and otherwise, $u_i \neq 0$. (ii) The second equation is deduced by Definition 1, that is $j \in \mathcal{N}(i)$, if $R_{i,j} \neq 0$. (iii) By the structure of $R \in \{0,1\}^{m \times n}$ with column degree d and with $R^\top_{*,\phi} R_{*,\phi} = dI_{|\phi|}$, $\phi = supp(u) \cup supp(v)$, it is easy to see that the columns of $R_{*,\phi}$ are orthogonal to each other, and equivalently, $\mathcal{N}(j_1) \cap \mathcal{N}(j_2) = \emptyset$, $\forall j_1 \neq j_2$ and j_1, $j_2 \in \phi$ (or $\in supp(u) \subset \phi$); the orthogonality property suggests that there exists only one column index $j \in \mathcal{N}(i) \cap supp(u)$ (and satisfying $R_{i,j} = 1$), $\forall i \in \mathcal{N}(supp(u))$, and this yields the third equation. (iv) The fourth equation is easily derived by $u_j \neq 0$, $j \in supp(u)$.

Combing the results of (11) and (12), it follows that $supp(u')$=$\mathcal{N}(supp(u))$, which indicates that the support of the projected data u' is the adjacent set of the support of the original data u. Similarly, the same result can also be derived for the other pair of data v, v', that is $supp(v')$=$\mathcal{N}(supp(v))$. Then the support intersection

ψ' of the two projected data u', v' can be expressed as

$$\begin{aligned}\psi' &\overset{1}{=} supp(u') \cap supp(v') \\ &\overset{2}{=} \mathcal{N}\left(supp(u)\right) \cap \mathcal{N}\left(supp(v)\right) \\ &\overset{3}{=} \mathcal{N}\left(supp(u) \cap supp(v)\right) \\ &\overset{4}{=} \mathcal{N}(\psi)\end{aligned} \tag{13}$$

which has the third equation derived by the orthogonality of $R_{*,\phi}$, implying $\mathcal{N}(j_1) \cap \mathcal{N}(j_2) = \emptyset$, $\forall j_1$, $j_2 \in \phi = supp(u) \cup supp(v)$. The result indicates that the support intersection ψ' of projected data u', v' is identical to the adjacent set of the support intersection ψ of original data u, v.

Given $\psi' = \mathcal{N}(\psi)$ in (13), we can further formulate (10) as

$$\begin{aligned}f_0(u')^\top f_0(v') &\overset{1}{=} \sum_{i \in \psi'} f_0(u'_i) f_0(v'_i) \\ &\overset{2}{=} \sum_{j \in \psi} \sum_{i \in \mathcal{N}(j)} f_0(u'_i) f_0(v'_i) \\ &\overset{3}{=} \sum_{j \in \psi} \sum_{i \in \mathcal{N}(j)} f_0(u_j) f_0(v_j) \\ &\overset{4}{=} d \cdot \sum_{j \in \psi} f_0(u_j) f_0(v_j) \\ &\overset{5}{=} d \cdot f_0(u)^\top f_0(v)\end{aligned} \tag{14}$$

for which the derivation is detailed as follows. (i) The second equation is derived by the result of (13), that is $\psi' = \mathcal{N}(\psi) = \bigcup_{j \in \psi} \mathcal{N}(j)$, with $\mathcal{N}(j_1) \cap \mathcal{N}(j_2) = \emptyset$, $\forall j_1 \neq j_2$ and j_1, $j_2 \in \phi$. (ii) The third equation results from the uniqueness of $j \in \mathcal{N}(i) \cap supp(u)$, provided $i \in \mathcal{N}(j)$, $j \in \psi \subset supp(u)$; and the details can be found in the analysis of the third equation of (12). (iii) The fourth equation is derived by $\mathcal{N}(j) = d$. The proof is complete. □

A.2 Proof of Theorem 2

Proof. The proof is similar to that of Theorem 1. First, we divide the element coordinates of the original data vectors u, v into two groups in terms of their element quantization $f_{\tau_1}(u_i)$, $f_{\tau_2}(v_i)$ equal to zero or not, in order to define the support union $\phi = supp(f_{\tau_1}(u)) \cup supp(f_{\tau_2}(v))$ and the intersection $\psi = supp(f_{\tau_1}(u)) \cap supp(f_{\tau_2}(v))$. In the similar way, we also define the support union ϕ' and intersection ψ' for the projected data u', v'. Then we need to identify the relation between ψ' and ψ. To achieve this, as in (11) and (12), we propose to determine the value of $f_{\tau_1}(u'_i)$ in terms of $i \in \mathcal{N}(supp(f_{\tau_1}(u)))$ or not. For the case of $i \notin \mathcal{N}(supp(f_{\tau_1}(u)))$, we have

$$\begin{aligned}f_{\tau_1}(u'_i) &= f_0\left(\sum_{j \in [n] \setminus supp(f_{\tau_1}(u))} R_{i,j} u_j\right) \\ &= 0\end{aligned} \tag{15}$$

since by the summation formula for geometric series, it can be deduced that $\tau_1 = \frac{|u^*_{k_1}| + |u^*_{k_1+1}|}{2}$ is greater than the absolute vale of the function input, under the condition of $|u^*_{i+1}|/|u^*_i| \leq e^{-\beta}$ and $\beta \geq \ln(2+\sqrt{3})$;

and for the other case of $i \notin \mathcal{N}\left(supp(f_{\tau_1}(u))\right)$, we can derive

$$\begin{aligned} & f_{\tau_1}(u_i') \\ & \overset{1}{=} f_{\tau_1}\left(\sum_{j \in supp(f_{\tau_1}(u))} R_{i,j}u_j + \sum_{j \in [n] \setminus supp(f_{\tau_1}(u_i))} R_{i,j}u_j\right) \\ & \overset{2}{=} f_{\tau_1}\left(u_{j=supp(f_{\tau_1}(u)))\cap\mathcal{N}(i)} + \sum_{j \in [n] \setminus supp(f_{\tau_1}(u_i))} R_{i,j}u_j\right) \\ & \overset{3}{=} f_{\tau_1}\left(u_{j=supp(f_{\tau_1}(u)))\cap\mathcal{N}(i)}\right) \\ & \overset{4}{\neq} 0 \end{aligned} \tag{16}$$

which has the third equation resulting from the relation of $\left|u_{j=supp(f_{\tau_1}(u)))\cap\mathcal{N}(i)}\right| > \left|\sum_{j \in [n] \setminus supp(f_{\tau_1}(u_i))} R_{i,j}u_j\right| + \tau_1$, while the relation can be derived using the same method as for (15). The above two results (15) and (16) are the major characteristics of the proof of Theorem 2, and the subsequent proof will proceed similarly as in Theorem 1, omitted here for brevity. □

A.3 Proof of Theorem 3

Proof. The condition of $R_{*,\phi}^\top R_{*,\phi} = dI_{|\phi|}$ means that $R_{*,j_1}^\top R_{*,j_2} = 0$ for $\forall\ j_1, j_2 \in \phi$, $j_1 \neq j_2$. In other words, the nonzero entries of any two columns of $R_{*,\phi}$ have no coordinates overlapping. By the distribution of the nonzero entries, we can express the probability as

$$\begin{aligned} Pr\{R_{*,\phi}^\top R_{*,\phi} = dI_{|\phi|}\} &= \frac{C_m^d C_{m-d}^d \cdots C_{m-(|\phi|-1)d}^d}{(C_m^d)^{|\phi|}} \\ &= \frac{[(m-d)!]^{|\phi|}}{(m!)^{|\phi|-1}(m-|\phi|d)!} \end{aligned}$$

Given m and ϕ, define $g(d; m, \phi) = Pr\{R_{*,\phi}^\top R_{*,\phi} = dI_{|\phi|}\}$. Then it can be derived that

$$\begin{aligned} \frac{g(d;m,\phi)}{g(d+1;m,\phi)} &= \frac{\frac{[(m-d)!]^{|\phi|}}{(m!)^{|\phi|-1}(m-|\phi|d)!}}{\frac{[(m-d+1)!]^{|\phi|}}{(m!)^{|\phi|-1}[(m-|\phi|(d+1)]!}} \\ &= \frac{(m-d)^{|\phi|}}{\prod_{\ell=0}^{|\phi|-1}(m-|\phi|d-\ell)} \\ &> 1, \end{aligned} \tag{17}$$

since $\frac{m-d}{m-|\phi|d-\ell} > 1$, $0 \leq \ell \leq |\phi|-1$. This indicates that $g(d; m, \phi)$ is a monotonically decreasing function, with its maximum value achieved by

$$\begin{aligned} g(d;m,\phi)|_{d=1} &= \frac{(m-1)!}{m^{|\phi|-1}(m-|\phi|)!} \\ &= \frac{\prod_{\ell=1}^{|\phi|-1}(m-\ell)}{m^{|\phi|-1}}. \end{aligned} \tag{18}$$

The proof is complete. □

A.4 Other experimental results

A.4.1 Distance preservation

In Figure 7, we calculate the distance variation rate by (8) for *binary* quantized projections. The results are consistent with our theoretical prediction: the distance variation rate of binary matrices tends to increase with the column degree d, particularly when the sparsity ratio k/n of the original data is sufficiently small.

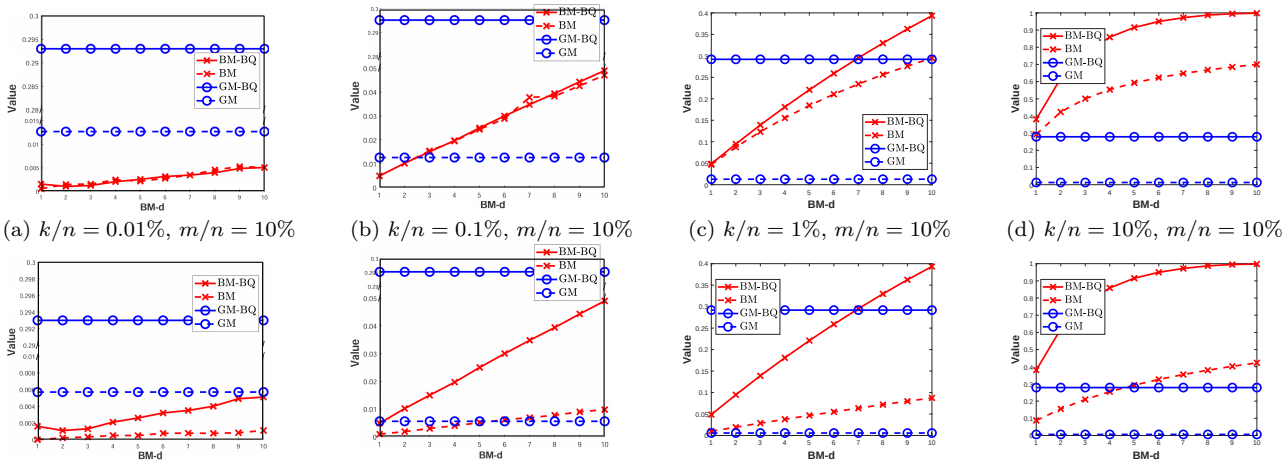

(a) $k/n = 0.01\%$, $m/n = 10\%$ (b) $k/n = 0.1\%$, $m/n = 10\%$ (c) $k/n = 1\%$, $m/n = 10\%$ (d) $k/n = 10\%$, $m/n = 10\%$

(e) $k/n = 0.01\%$, $m/n = 50\%$ (f) $k/n = 0.1\%$, $m/n = 50\%$ (g) $k/n = 1\%$, $m/n = 50\%$ (h) $k/n = 10\%$, $m/n = 50\%$

Figure 7: Distance variation rate for the binary-quantized (BQ) (and non-quantized) projections of the generated data, with three different feature sparsity ratios $k/n = 0.01\%$, 0.1%, 1% and 10%, using two projection matrices: the Gaussian matrix (GM) and the binary matrix (BM) with varying column degree BM-d $\in [1, 10]$, under two projection ratios $m/n = 10\%$ and 50%. Note the smaller the distance variation rate, the better the distance preservation.

A.4.2 Classification

In Figure 8, we conduct the **SVM** classification on the **ternary**-quantized projections of YaleB (DWT), and conduct the **KNN** classification on the **binary**-quantized projections of CIFAR10 (AlexNet) and Mini-ImageNet (VGG16), respectively, in Figures 9 and 10. The classification results in Figures 8-10 demonstrate a performance trend that aligns with our theoretical prediction: the extremely sparse binary matrix with column degree $d = 1$ can achieve superior or at least comparable performance to other denser matrices with larger d values.

A.4.3 Clustering

In Figures 11-13 and Figures 14-16, we respectively examine the k-means clustering performance on the **ternary** and **binary**-quantized projections of YaleB (DWT), CIFAR10 (AlexNet) and Mini-ImageNet (VGG16). The results are consistent with our theoretical prediction: the extremely sparse binary matrix with column degree $d = 1$ can achieve superior or at least comparable performance to other denser matrices with larger d values.

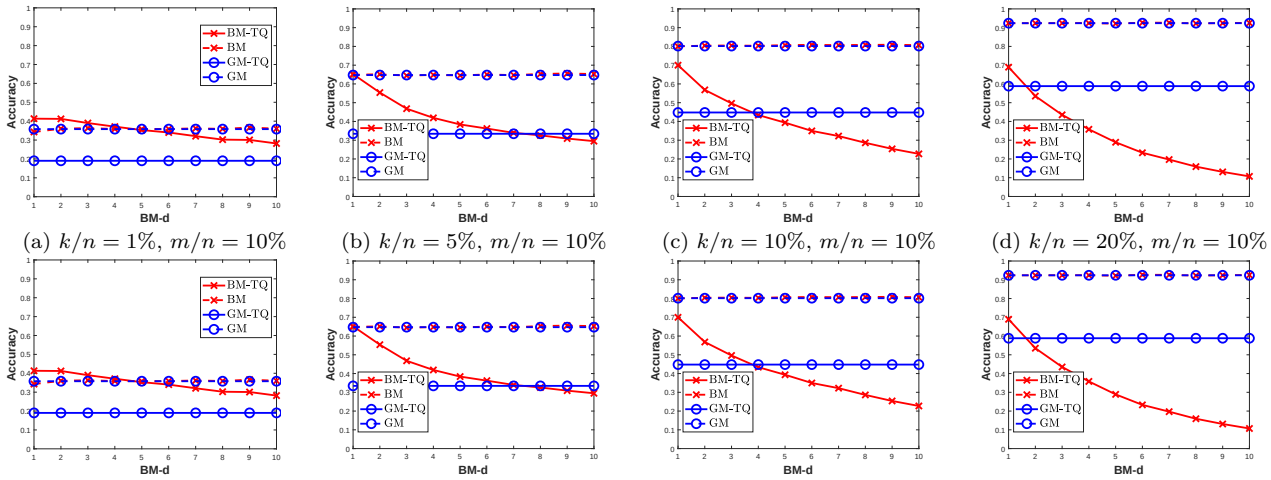

(a) $k/n = 1\%$, $m/n = 10\%$ (b) $k/n = 5\%$, $m/n = 10\%$ (c) $k/n = 10\%$, $m/n = 10\%$ (d) $k/n = 20\%$, $m/n = 10\%$

(e) $k/n = 1\%$, $m/n = 50\%$ (f) $k/n = 5\%$, $m/n = 50\%$ (g) $k/n = 10\%$, $m/n = 50\%$ (h) $k/n = 20\%$, $m/n = 50\%$

Figure 8: SVM classification accuracy for the ternary-quantized (TQ) (and non-quantized) projections of the exactly sparse features of YaleB (DWT), with three different feature sparsity ratios $k/n = 1\%$, 5%, 10% and 20%, using two projection matrices: the Gaussian matrix (GM) and the binary matrix (BM) with varying column degree BM-d $\in [1, 10]$, under two projection ratios $m/n = 10\%$ and 50%.

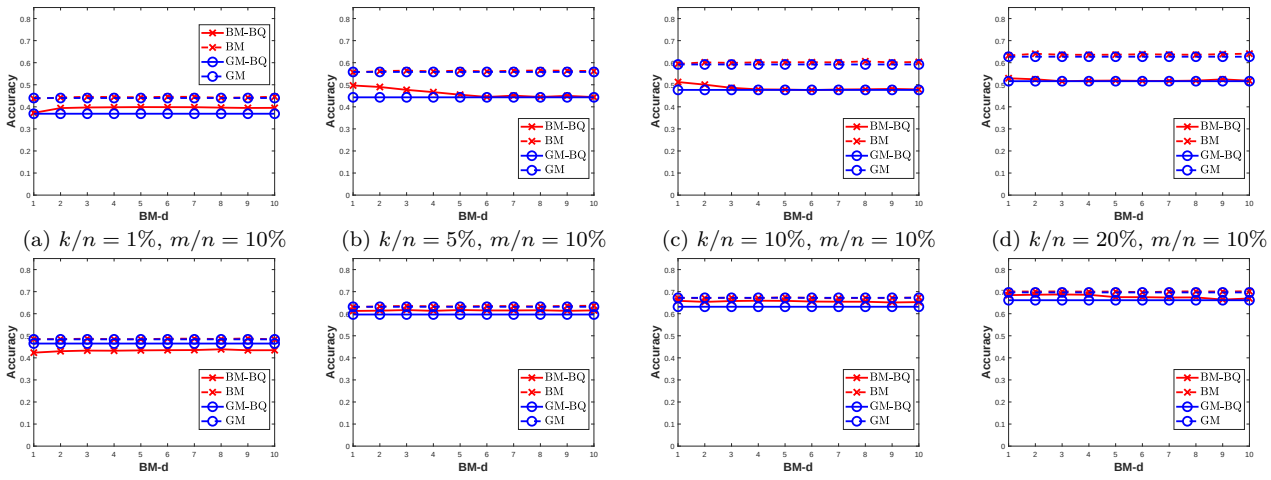

(a) $k/n = 1\%$, $m/n = 10\%$ (b) $k/n = 5\%$, $m/n = 10\%$ (c) $k/n = 10\%$, $m/n = 10\%$ (d) $k/n = 20\%$, $m/n = 10\%$

(e) $k/n = 1\%$, $m/n = 50\%$ (f) $k/n = 5\%$, $m/n = 50\%$ (g) $k/n = 10\%$, $m/n = 50\%$ (h) $k/n = 20\%$, $m/n = 50\%$

Figure 9: Classification accuracy for the binary-quantized (BQ) (and non-quantized) projections of the exactly sparse features of CIFAR10 (AlexNet), with three different feature sparsity ratios $k/n = 1\%$, 5%, 10% and 20%, using two projection matrices: the Gaussian matrix (GM) and the binary matrix (BM) with varying column degree BM-d $\in [1, 10]$, under two projection ratios $m/n = 10\%$ and 50%.

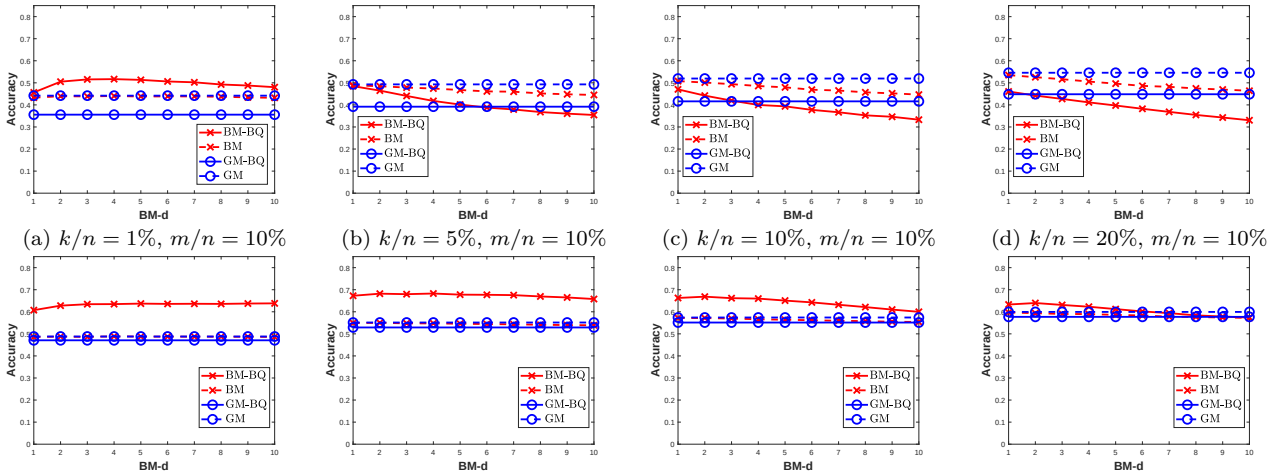

(a) $k/n = 1\%$, $m/n = 10\%$ (b) $k/n = 5\%$, $m/n = 10\%$ (c) $k/n = 10\%$, $m/n = 10\%$ (d) $k/n = 20\%$, $m/n = 10\%$

(e) $k/n = 1\%$, $m/n = 50\%$ (f) $k/n = 5\%$, $m/n = 50\%$ (g) $k/n = 10\%$, $m/n = 50\%$ (h) $k/n = 20\%$, $m/n = 50\%$

Figure 10: Classification accuracy for the binary-quantized (BQ) (and non-quantized) projections of the exactly sparse features of Mini-ImageNet (VGG16), with three different feature sparsity ratios $k/n = 1\%$, 5%, 10% and 20%, using two projection matrices: the Gaussian matrix (GM) and the binary matrix (BM) with varying column degree BM-d $\in [1, 10]$, under two projection ratios $m/n = 10\%$ and 50%.

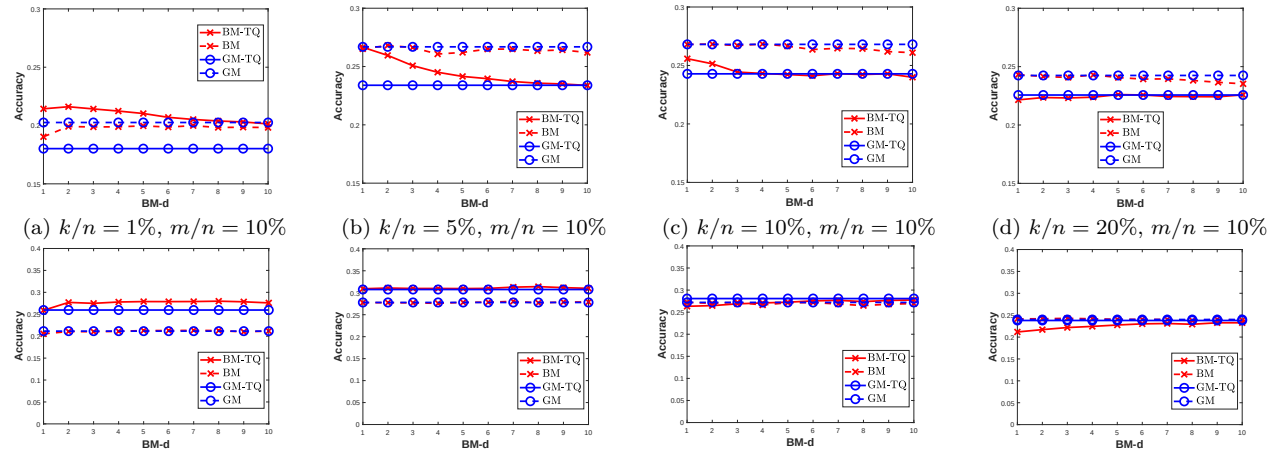

(a) $k/n = 1\%$, $m/n = 10\%$ (b) $k/n = 5\%$, $m/n = 10\%$ (c) $k/n = 10\%$, $m/n = 10\%$ (d) $k/n = 20\%$, $m/n = 10\%$

(e) $k/n = 1\%$, $m/n = 50\%$ (f) $k/n = 5\%$, $m/n = 50\%$ (g) $k/n = 10\%$, $m/n = 50\%$ (h) $k/n = 20\%$, $m/n = 50\%$

Figure 11: Clustering accuracy for the ternary-quantized (TQ) (and non-quantized) projections of the exactly sparse features of YaleB (DWT), with three different feature sparsity ratios $k/n = 1\%$, 5%, 10% and 20%, using two projection matrices: the Gaussian matrix and the binary matrix with varying column degree BM-d $\in [1, 10]$, under two projection ratios $m/n = 10\%$ and 50%.

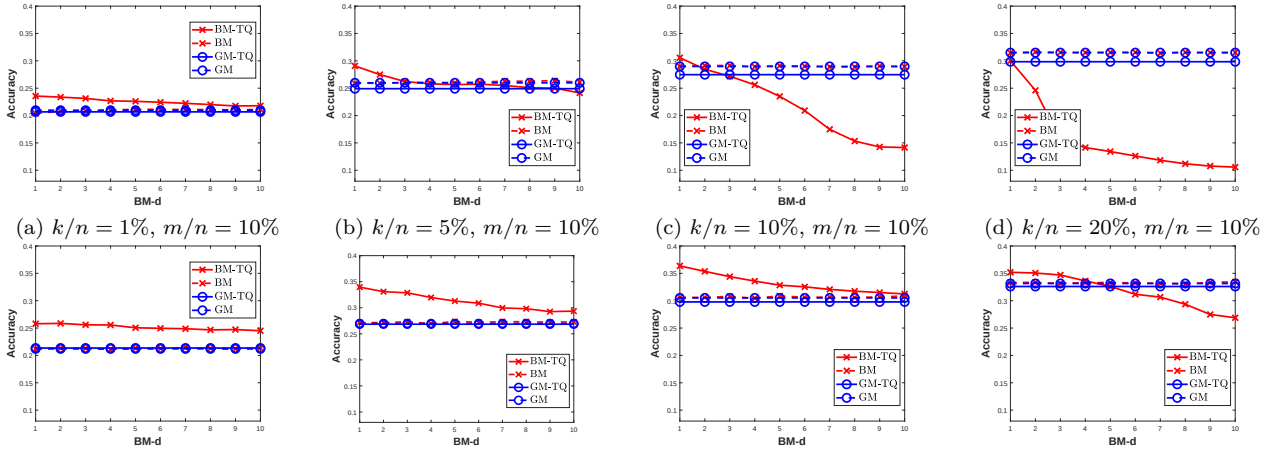

(a) $k/n = 1\%$, $m/n = 10\%$ (b) $k/n = 5\%$, $m/n = 10\%$ (c) $k/n = 10\%$, $m/n = 10\%$ (d) $k/n = 20\%$, $m/n = 10\%$

(e) $k/n = 1\%$, $m/n = 50\%$ (f) $k/n = 5\%$, $m/n = 50\%$ (g) $k/n = 10\%$, $m/n = 50\%$ (h) $k/n = 20\%$, $m/n = 50\%$

Figure 12: Clustering accuracy for the ternary-quantized (TQ) (and non-quantized) projections of the exactly sparse features of CIFAR10 (AlexNet), with three different feature sparsity ratios $k/n = 1\%$, 5%, 10% and 20%, using two projection matrices: the Gaussian matrix and the binary matrix with varying column degree BM-d $\in [1, 10]$, under two projection ratios $m/n = 10\%$ and 50%.

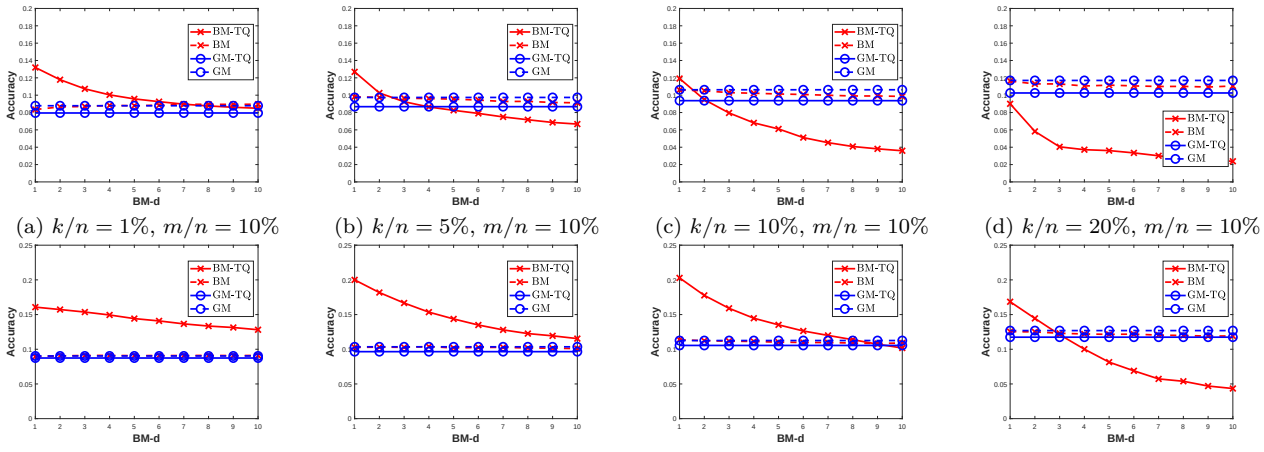

(a) $k/n = 1\%$, $m/n = 10\%$ (b) $k/n = 5\%$, $m/n = 10\%$ (c) $k/n = 10\%$, $m/n = 10\%$ (d) $k/n = 20\%$, $m/n = 10\%$

(e) $k/n = 1\%$, $m/n = 50\%$ (f) $k/n = 5\%$, $m/n = 50\%$ (g) $k/n = 10\%$, $m/n = 50\%$ (h) $k/n = 20\%$, $m/n = 50\%$

Figure 13: Clustering accuracy for the ternary-quantized (TQ) (and non-quantized) projections of the exactly sparse features of Mini-ImageNet (VGG16), with three different feature sparsity ratios $k/n = 1\%$, 5%, 10% and 20%, using two projection matrices: the Gaussian matrix and the binary matrix with varying column degree BM-d $\in [1, 10]$, under two projection ratios $m/n = 10\%$ and 50%.

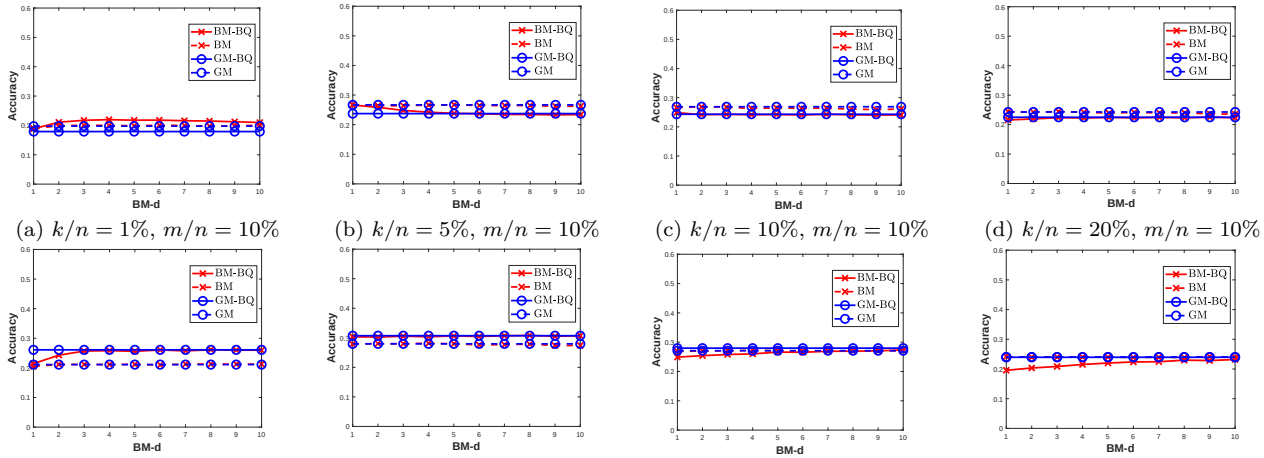

(a) $k/n = 1\%$, $m/n = 10\%$ (b) $k/n = 5\%$, $m/n = 10\%$ (c) $k/n = 10\%$, $m/n = 10\%$ (d) $k/n = 20\%$, $m/n = 10\%$

(e) $k/n = 1\%$, $m/n = 50\%$ (f) $k/n = 5\%$, $m/n = 50\%$ (g) $k/n = 10\%$, $m/n = 50\%$ (h) $k/n = 20\%$, $m/n = 50\%$

Figure 14: Clustering accuracy for the binary-quantized (BQ) (and non-quantized) projections of the exactly sparse features of YaleB (DWT), with three different feature sparsity ratios $k/n = 1\%$, 5%, 10% and 20%, using two projection matrices: the Gaussian matrix and the binary matrix with varying column degree BM-d $\in [1, 10]$, under two projection ratios $m/n = 10\%$ and 50%.

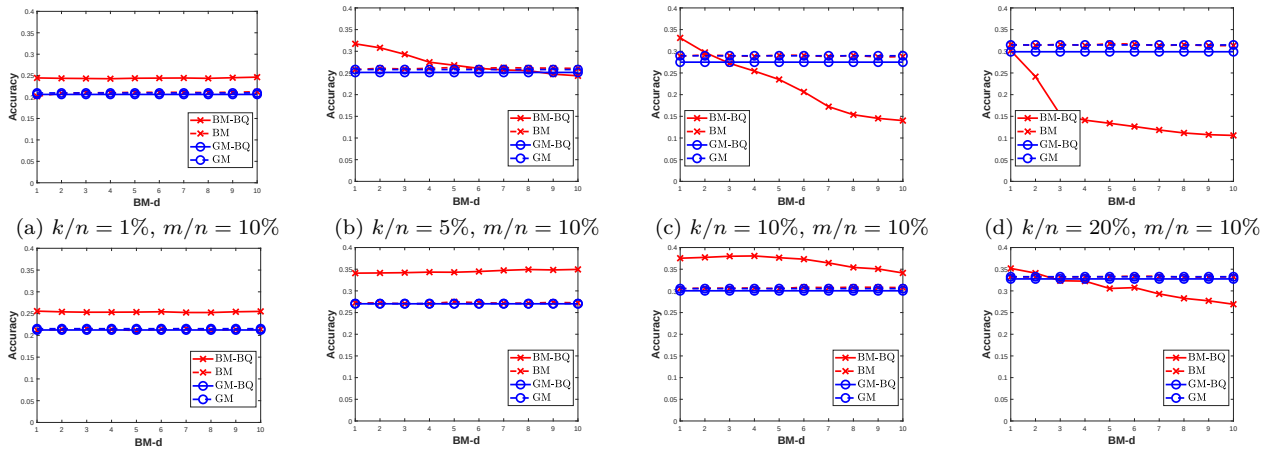

(a) $k/n = 1\%$, $m/n = 10\%$ (b) $k/n = 5\%$, $m/n = 10\%$ (c) $k/n = 10\%$, $m/n = 10\%$ (d) $k/n = 20\%$, $m/n = 10\%$

(e) $k/n = 1\%$, $m/n = 50\%$ (f) $k/n = 5\%$, $m/n = 50\%$ (g) $k/n = 10\%$, $m/n = 50\%$ (h) $k/n = 20\%$, $m/n = 50\%$

Figure 15: Clustering accuracy for the binary-quantized (BQ) (and non-quantized) projections of the exactly sparse features of CIFAR10 (AlexNet), with three different feature sparsity ratios $k/n = 1\%$, 5%, 10% and 20%, using two projection matrices: the Gaussian matrix and the binary matrix with varying column degree BM-d $\in [1, 10]$, under two projection ratios $m/n = 10\%$ and 50%.

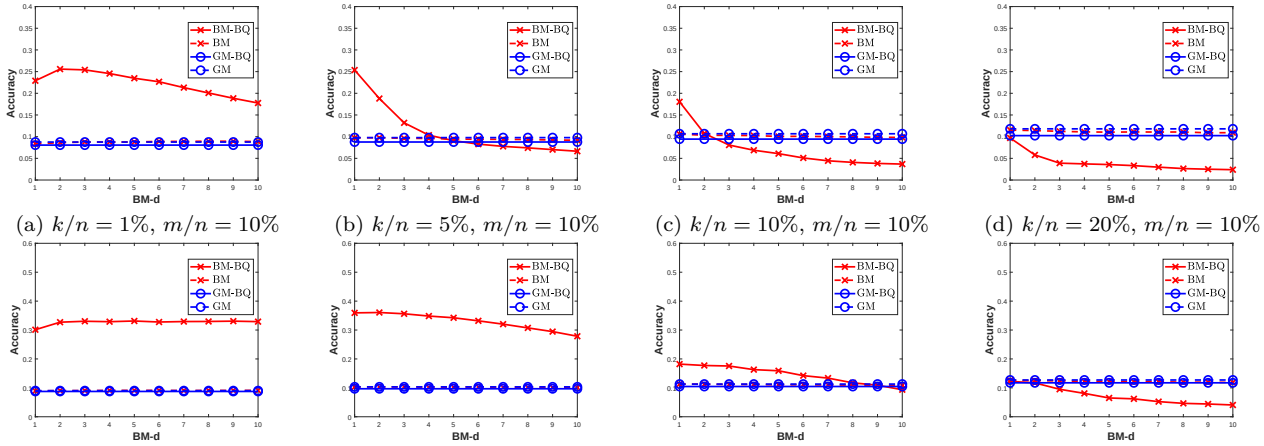

(a) $k/n = 1\%$, $m/n = 10\%$ (b) $k/n = 5\%$, $m/n = 10\%$ (c) $k/n = 10\%$, $m/n = 10\%$ (d) $k/n = 20\%$, $m/n = 10\%$

(e) $k/n = 1\%$, $m/n = 50\%$ (f) $k/n = 5\%$, $m/n = 50\%$ (g) $k/n = 10\%$, $m/n = 50\%$ (h) $k/n = 20\%$, $m/n = 50\%$

Figure 16: Clustering accuracy for the binary-quantized (BQ) (and non-quantized) projections of the exactly sparse features of Mini-ImageNet (VGG16), with three different feature sparsity ratios $k/n = 1\%$, 5%, 10% and 20%, using two projection matrices: the Gaussian matrix and the binary matrix with varying column degree BM-d $\in [1, 10]$, under two projection ratios $m/n = 10\%$ and 50%.